ACS APPLIED NANO MATERIALS

www.acsanm.org Letter

Size- and Phase-Controlled Nanometer-Thick β-Ga_2O_3 Films with Green Photoluminescence for Optoelectronic Applications

Nanthakishore Makeswaran, Debabrata Das, Vishal Zade, Paul Gaurav, V. Shutthanandan, Susheng Tan,* and C. V. Ramana*

Cite This: *ACS Appl. Nano Mater.* 2021, 4, 3331−3338 Read Online

ACCESS | Metrics & More | Article Recommendations

ABSTRACT: Realization and optimization of the tunable/enhanced optical properties are critical to further advancing the fields of optoelectronics, photonics, and nanoelectronics. In this context, here, we demonstrate green-emission characteristics with a ∼30-fold enhancement in selectively engineered nanocrystalline Ga_2O_3 with control over the size, phase, and interface nanostructure. Pulsed-laser-deposited β-phase Ga_2O_3 films with an average crystallite size of ∼9 nm along with a highly dense, close-compact nanocolumnar structure with the lowest possible defect density facilitate the 30-fold enhancement in the photoluminescence (PL) intensity in the green region. Enhanced PL emission in the optimized, engineered nanoarchitecture sheds light on the design of Ga_2O_3 materials for promising future optoelectronic/photocatalytic applications.

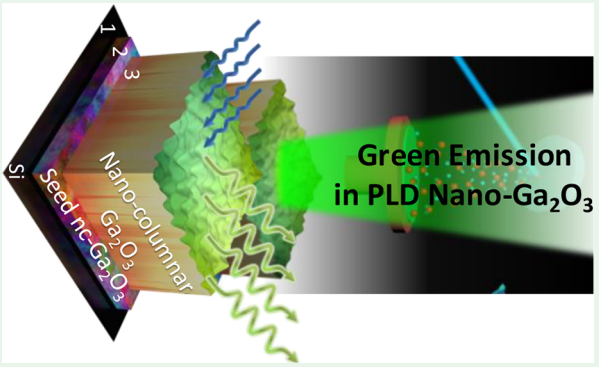

KEYWORDS: *Ga_2O_3, nanocrystalline films, pulsed-laser deposition, selective nanocrystallization, optical properties, green emission*

INTRODUCTION

Gallium oxide (Ga_2O_3) was first introduced in the year closer to 1900. Thus, the novel metal oxide had been in the outskirts of mainstream scientific and engineering research for over a century before the genesis of electronic revolution. For the last few decades, Ga_2O_3 has been scrutinized intensely and more rigorously to understand its mesmerizing thermal stability[1] and wide-band-gap semiconducting ability.[2−6] Typically, Ga_2O_3 shows six different polymorphs,[7,8] such as α, β, γ, δ, ε, and κ. However, β-Ga_2O_3 is the only stable phase throughout the whole temperature range.[8] It has monoclinic crystal structure and crystallizes in the $C2/m$ space group. Ga_2O_3 places on record in second place in terms of its direct band gap of ∼4.9 eV,[8] which is only next to diamond among all available materials with the highest band gaps. Also, it shows anisotropic thermal conductivity through different crystal orientations,[8,9] which is why it is very challenging to grow such defect-free bulk crystals and nanostructures.

β-Ga_2O_3 has already been established for its potential in multidimensional functionality, which makes these materials interesting for numerous technological applications, such as catalysis (in electrocatalysis and photoelectrocatalysis), phosphor, chemical sensor, gas sensor, photovoltaic, water splitting, CO_2 reduction, Schottky diode, field-effect transistor, neuromorphic device, electrode for a storage device, and, most recently, lithium batteries.[4,10−17] However, the pioneering novelty of this astonishing oxide material lies in the field of power electronic devices, deep-UV optoelectronic and photonic devices, and sensors.[15] Additionally, there is an increasing trend of using a Ga_2O_3/Ga−In-based eutectic interface to probe self-assembled organic/inorganic monolayers for molecular-based devices.[18−20] An ultrawide band gap along with advancements made for high-quality β-Ga_2O_3 has already procured many state-of-the-art scientific breakthroughs. However, β-Ga_2O_3 and related materials continue to attract the scientific and engineering community along with technologists, and policy makers continue to exploit their full potential, especially as an alternative competitor to the mainstream electronic, optoelectronic, and photonic industries. Furthermore, new applications involving Ga_2O_3 and its related compounds are continuously evolving, which indicates the promise for future novel technology development. For instance, while there is significant interest in overcoming the technological challenges in the design and development of large-area inorganic−organic thermoelectrics by means of engineering the materials at the molecular scale, recent studies

Received: February 5, 2021
Accepted: March 18, 2021
Published: March 26, 2021

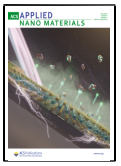

indicate promise for such thermoelectrics based on Ga/Ga_2O_3 compounds.[18−20]

β-Ga_2O_3 thin films can be deposited by means of numerous physical and chemical methods. Metal−organic chemical vapor deposition, molecular beam epitaxy, vapor phase epitaxy, Czochralski, etc.,[2,21−24] fall into the category of highly expensive epitaxial growth processes, where we can control the dynamics very precisely and obtain material of the highest possible quality. All of these processes are dedicated to a few very specific highly delicate device applications, where the community cannot compromise the material quality over pricing. On the contrary, there are many other low-cost processes, like chemical vapor deposition, sputtering, pulsed-laser deposition (PLD), electrospinning, chemical bath deposition, etc.,[1,11,15,16,19,20,25,26] that can be incorporated into relatively low-cost applications for the mass. Especially, these chemical and physical methods were employed to design various nanoarchitectures, such as columnar nanostructures, vertical nanopillar, inclined nanopillar, fractal, nanohelix, zigzag nanopillars, etc., which have proven to be very promising for electronics, optoelectronics, and photocatalysis. However, the controlled growth of such complex nanocrystalline structures with precise size control and phase stability, while deriving enhanced properties and performance, is always very challenging. In this context, here in this work, using conventional PLD, we demonstrate a close-compact nano-columnar β-Ga_2O_3 film, decorated with nanocrystalline surface morphology, by using anisotropic thermal-conductivity-assisted selective unidirectional growth of β-Ga_2O_3 nanocrystals. Most importantly, we demonstrate the green emission characteristic in selectively and precisely engineered β-Ga_2O_3 nanocrystalline films, where size, shape, and phase control enable such optical features or phenomena, which is otherwise not possible in intrinsic Ga_2O_3 materials.

The luminescence in β-Ga_2O_3 has been widely investigated in the recent past.[25−27] A deeper understanding of the effect of doping into β-Ga_2O_3 to derive the desired properties is the primary outcome. The conglomeration of research results with respect to photoluminescence (PL) in β-Ga_2O_3, variable dopants, and their concentrations was used as a primary means to derive the emission with a specific color in the visible region. Zhou et al.[27] reported the ultraviolet (UV) and red-emission PL bands at ∼3.40 and ∼1.78 eV, respectively, in β-Ga_2O_3 nanostructures. These nanostructures were arranged in a core−shell structure, where the crystalline core is associated with an amorphous shell. In fact, both blue- and green-emission characteristics were observed in β-Ga_2O_3 previously. Recombination of the charge carriers trapped by the O and Ga vacancies, leading to deep donor and acceptor states, respectively, has been proposed as the origin of the blue PL band. On the other hand, much controversy exists in terms of the red- and green-emission characteristics in β-Ga_2O_3. While different explanations exist for the UV and red emission, the green emission in β-Ga_2O_3 derived by means of doping was commonly observed in doped β-Ga_2O_3 samples. In this context, here in this report, we demonstrate an approach to obtaining green-emission characteristics with a 30-fold enhancement in selectively engineered nanocrystalline Ga_2O_3 films without any need for dopants, epitaxial structure, or quite expensive equipment for fabrication. The green-emission characteristics in nanocrystalline β-Ga_2O_3 films with a crystallite size of ∼9 nm are made possible by means of control of the size, phase, and interface of the nanostructure, where highly dense, close-compact nanocolumnar interface microstructures were the characteristic features that were accounted for this observation.

MATERIALS AND METHODS

Ga_2O_3 films were deposited onto well-cleaned silicon (100) substrates. The background chamber pressure was 10^{-7} Torr before introducing oxygen inside the growth chamber. A KrF excimer laser with a wavelength of 248 and with 220 mJ cumulative energy was used to ablate the target. The laser beam of pulses with a 5 Hz pulse frequency was used to excite the rotating Ga_2O_3 target. The target-to-substrate distance was maintained at 45 mm. The in situ oxygen partial pressure was kept at 50 mTorr during deposition of Ga_2O_3. All of the parameters were precalibrated to achieve the best possible film quality. Using the sintered Ga_2O_3 target and high-energy laser processing (Figure 1a) under the optimum thermodynamic

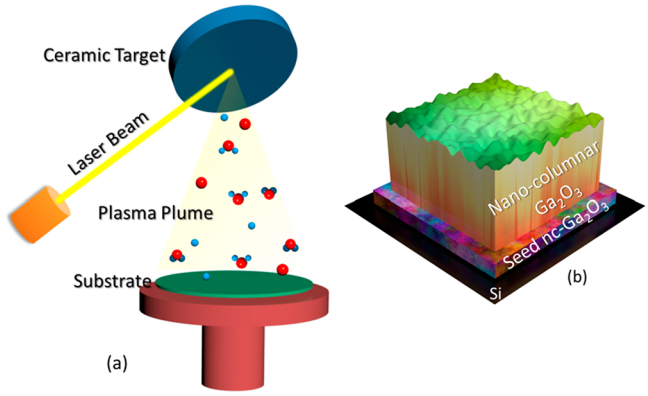

Figure 1. (a) Schematic diagram showing PLD of β-Ga_2O_3. (b) Schematic of a nanostructured Ga_2O_3 thin film on Si.

conditions was the key approach that was employed to realize high-quality β-Ga_2O_3 films. Controlled ablation of the Ga_2O_3 PLD target generated a high-energy plasma plume containing micro- and nanoscale molecules and/or elemental Ga/O adatoms. The energetic particles, thus produced, were directed toward the substrate under a specific oxygen environment (Figure 1a) for reactive Ga_2O_3 film growth. Under the optimum deposition conditions, the expected nanostructured Ga_2O_3 film is schematically shown in Figure 1b. The number of laser pulses was kept at 2000, which produced a film thickness of 150−250 nm, depending on the substrate temperature. Although the in situ chamber pressure during the growth of nanocolumnar β-Ga_2O_3 was relatively high, there was a clear reduction of the film thickness with higher substrate temperature, which directly implies the presence of adatom outdiffusion during the growth process.

X-ray diffraction (XRD) measurements were performed on the Ga_2O_3 thin films using a Rigaku Smartlab diffractometer in 1D mode with a HyPix 3000 high-energy-resolution 2D hybrid pixel array detector. The Nanosurf atomic force microscopy (AFM) system is used to give high-resolution topography, deflection, and phase-contrast data. Transmission electron microscopy (TEM) characterization was carried out on a Thermo Scientific (formerly FEI) Titan Themis 200 G2 probe aberration-corrected system equipped with a SuperX energy-dispersive X-ray spectrometer and operated at 200 kV. The TEM specimens were prepared using a FEI Scios focused ion beam (FIB) and scanning electron microscopy dual-beam system following a standard protocol for TEM specimen preparation. First, using an electron beam at 5 kV and 1.6 nA, a thin C protection layer of 15 μm × 2 μm was deposited on the Ga_2O_3 film grown on a Si substrate, and then a 15 μm × 2 μm × 2 μm Pt protection film was deposited on top of the C protection layer at 30 kV and 300 pA, followed by rough cutting, cleaning cut, J-cut, and lamellae transfer out of the substrate to a TEM grid. The final thinned specimen of

https://doi.org/10.1021/acsanm.1c00378
ACS Appl. Nano Mater. 2021, 4, 3331−3338

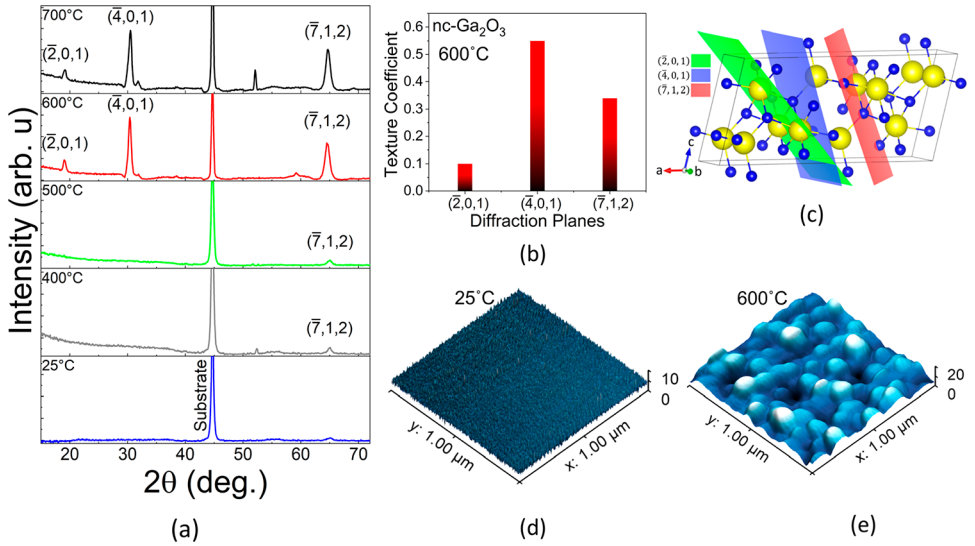

Figure 2. (a) $\theta/2\theta$ XRD of as-grown gallium oxide thin films with increasing in situ substrate temperature, showing the evolution of amorphous gallium oxide into nanocrystalline β-Ga_2O_3. The peaks noted are $(\bar{2}01)$, $(\bar{4}01)$, and $(\bar{7}12)$. (b) Texture coefficient of the corresponding diffraction planes, deposited at higher substrate temperature, where $(\bar{4}01)$ shows the highest among all of them. (c) Schematic of a monoclinic β-Ga_2O_3 unit cell, with the three diffraction planes contributing to the observed XRD peaks. (d) 1×1 μm^2 surface morphology of amorphous Ga_2O_3 and (e) highly oriented nanocrystalline β-Ga_2O_3 film.

about 80 nm was further FIB-cleaned at 5 kV and 48 pA and at 2 kV and 27 pA, respectively, to remove excess amorphotized and contaminated layers. TEM data processing, if any, was carried out using the relevant offline data processing software from Thermo Scientific. Fiji *ImageJ* was also employed to run radial profile analysis of selective area electron diffraction (SAED). X-ray photoelectron spectroscopy (XPS) scans of the PLD gallium oxide films were obtained with a Kratos Axis Ultra DLD spectrometer equipped with an Al Kα monochromatic X-ray source (1486.6 eV) and a high-resolution hemispherical analyzer. We adopted previously established procedures and methods for XPS characterization of gallium oxide and related materials.[1]

The optical absorption behavior of as-grown samples was scrutinized through diffuse-reflectance spectroscopy. A Jasco V-770 UV−visible spectrophotometer, with an optical resolution of 0.3 nm, was employed to capture the spectrum. For PL measurements, the as-grown Ga_2O_3 thin-film samples were excited with a 80 MHz 100 fs Ti:sapphire laser, equipped with an additional third-harmonic generator. The excitation energy and cumulative power were 180 nm and 10 W/cm^2, respectively, and were kept constant. The emitted photons were subjected to a monochromator with 0.02 nm resolution, followed by a photomultiplier tube detector.

RESULTS AND DISCUSSION

The crystal structure, phase stabilization and strain (if any), and morphology data of the PLD Ga_2O_3 films are presented in Figure 2. The XRD data of PLD Ga_2O_3 films (Figure 2a) indicate the information on the crystal structure and phase. The sequence of structural transformations induced as a function of the deposition temperature (T_s) can also be noted. It is evident that XRD peaks with appreciable intensity can be seen only in the Ga_2O_3 samples deposited at $T_s \geq 600$ °C. On the other hand, Ga_2O_3 films deposited at $T_s < 600$ °C are all amorphous, as is evident from the diffuse nature of the XRD patterns. An amorphous-to-crystalline structural transformation can be noted in Ga_2O_3 films when T_s is 600 °C. The Ga_2O_3 films deposited at T_s = 600−700 °C correspond to a monoclinic crystal structure, which has been identified to be β-Ga_2O_3 existing in the $C2/m$ space group. However, both of them show the presence of slightly varying lattice parameters and strain profiles. The average crystallite size calculated using the Scherrer equation is ∼9 nm, which is more or less the same for Ga_2O_3 films deposited at T_s = 600−700 °C.

The XRD results also indicate that the PLD nanocrystalline β-Ga_2O_3 samples exhibit the preferred orientation. The films deposited on Si(100) substrates clearly show textured growth, which is seen in the detailed quantitative analysis (Figure 2b). While the three diffraction planes with the appreciable intensity identified are $(\bar{2}01)$, $(\bar{4}01)$, and $(\bar{7}12)$ (Figure 2c), the PLD Ga_2O_3 films exhibit $(\bar{4}01)$ texturing. The degree of texturing can be understood from the texture coefficient (Figure 2b), which is relatively higher for β-Ga_2O_3 films deposited at 600−700 °C. The kinetics and thermodynamic processes involved in finding the most stable texture development are related to the contributing effects of the atomic influx and the minimum energy for that particular synthesis condition. Increasing T_s provides the additional kinetic energy, leading to the growth of more random crystals. A similar temperature-dependent trend was observed earlier, where after a certain critical substrate temperature it showed a drastic phase transition from amorphous-to-nanocrystalline material formation.

Parts d and e of Figure 2 show the morphology fingerprints of amorphous and nanocrystalline PLD Ga_2O_3 films, respectively. The nanocrystalline Ga_2O_3 films exhibit higher root-mean-square (RMS) roughness compared to those amorphous films. Also, for nanocrystalline PLD Ga_2O_3 films, the Gaussian-type grain-size distribution characteristics prevail, whereas the other samples exhibit almost a flat surface without any signature of cluster formation. These results corroborate with XRD analyses in distinguishing the crystalline versus amorphous PLD Ga_2O_3 films. The increased RMS roughness values can be due to the self-assembled conical nanotextures, with dimensions of 10−20 nm, on the front surface. Such morphological features promote the algorithm of multiple reflection and absorption, which results into better photon absorption.[29]

https://doi.org/10.1021/acsanm.1c00378
ACS Appl. Nano Mater. 2021, 4, 3331−3338

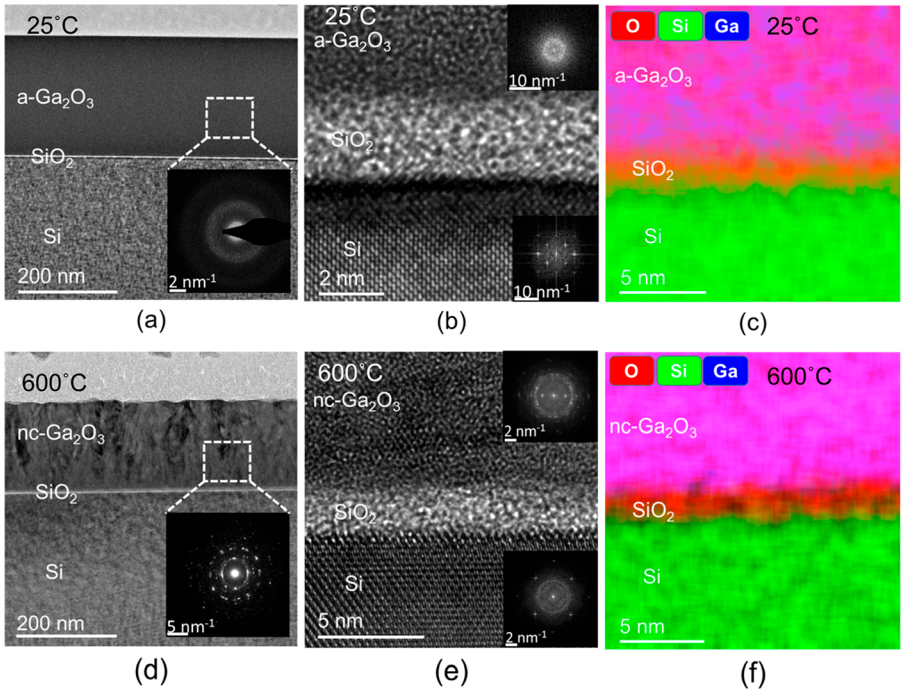

Figure 3. Cross-sectional TEM imaging analyses of Ga_2O_3 films. The TEM images of amorphous Ga_2O_3 (a–c) and nanocrystalline Ga_2O_3 (d–f) films are shown along with the corresponding elemental color mapping. In situ diffraction patterns provide evidence for the amorphous and nanocrystalline nature of the samples. For nanocrystalline Ga_2O_3, the TEM data (image d) shows close-compact nanocolumnar growth after the thin β-Ga_2O_3 seed layer.

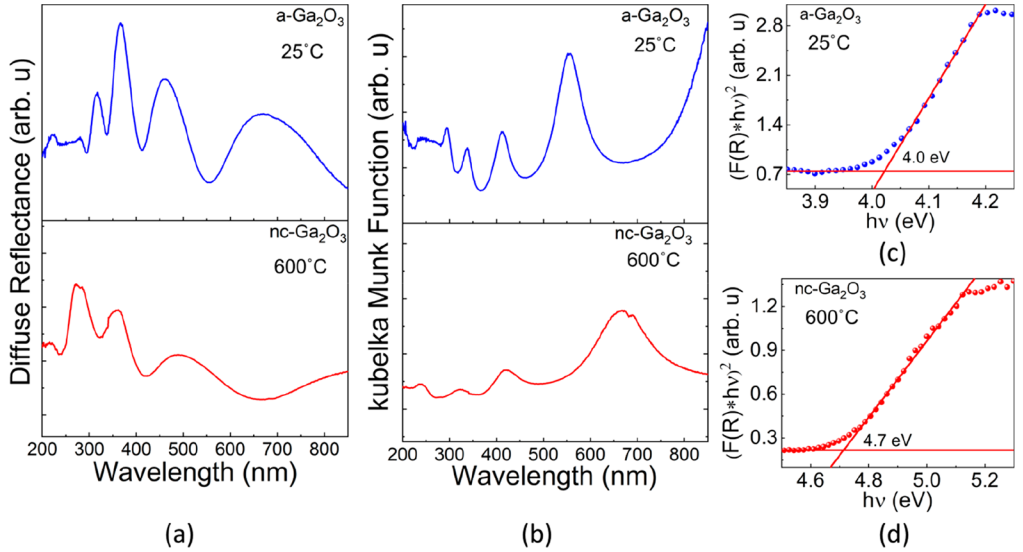

Figure 4. Optical property analyses of amorphous and nanocrystalline Ga_2O_3 films. (a) Diffuse-reflectance spectra obtained for Ga_2O_3 samples at a perpendicular photon incident mode. Assertively, amorphous Ga_2O_3 shows higher interference fringes than nanocrystalline Ga_2O_3 films. (b) Kubelka–Munk function of the corresponding amorphous and nanocrystalline Ga_2O_3 films. The Kubelka–Munk function derived from the reflectance data clearly indicates significant differences in the respective Ga_2O_3 thin-film samples. (c and d) Tauc plots of amorphous and nanocrystalline Ga_2O_3 films. The band-edge absorption difference can be noted if amorphous Ga_2O_3 is compared to nanocrystalline Ga_2O_3.

The structural quality and interface nanostructure of Ga_2O_3 films further evidenced in TEM analyses are presented in Figure 3. The data shown are the representative survey and high-resolution TEM (HRTEM) images and SAED patterns from the specifically selected regions of the Ga_2O_3 film–Si substrate. Additionally, the fast Fourier transfer spectra are also shown as insets in the corners of the relevant HRTEM images. High-quality interface structures are manifested for all of the PLD Ga_2O_3 films, which were found to be uniform with sharp surfaces. No significant diffusion of Ga_2O_3 into the substrate interface was observed. Corroborating with the XRD results, the HRTEM and SAED analyses further confirm the formation of amorphous and nanocrystalline Ga_2O_3 films depending on T_s. Apparently, fabrication at elevated substrate temperature (600–700 °C) accelerates the nucleation and growth of β-Ga_2O_3. Preferential texturing along $(\bar{4}01)$ was confirmed by both XRD (Figure 2) and SAED (Figure 3), while structural

https://doi.org/10.1021/acsanm.1c00378
ACS Appl. Nano Mater. 2021, 4, 3331–3338

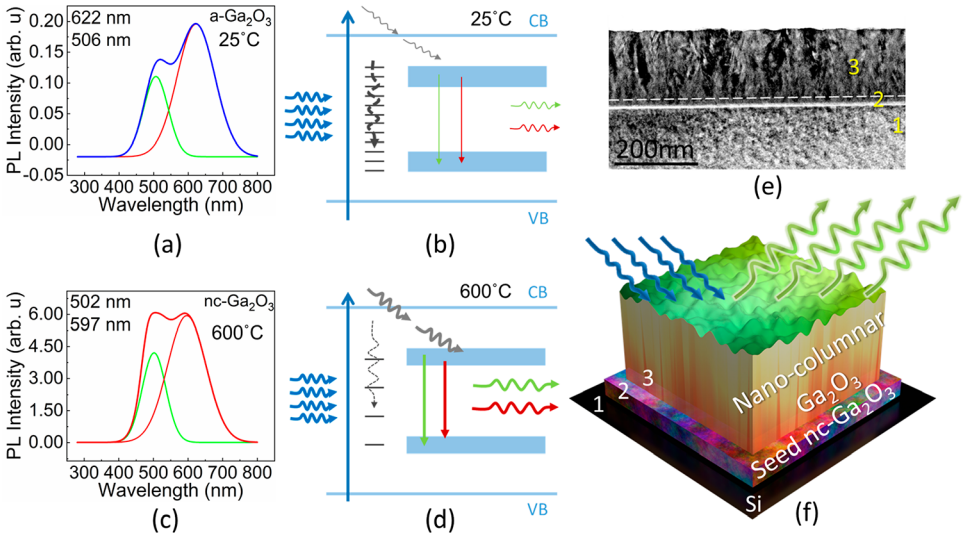

Figure 5. Room temperature PL spectra of amorphous (a) and nanocrystalline (c) Ga_2O_3 films. (b and d) Corresponding transitions of photoexcited electrons. Evidently, there is a giant jump in the photoextraction efficiency, with a moderate blue shift between the donor−acceptor energy states. (e) Cross-sectional transmission electron microscope image of close-compact nanocolumnar β-Ga_2O_3 thin film, showing three stages of the growth process, Si substrate 1, nanocrystalline seed layer 2, nanocolumnar β-Ga_2O_3 3. (f) Schematic of a close-compact nanocolumnar β-Ga_2O_3 on top of a randomly oriented seed β-Ga_2O_3 layer on the Si substrate, facilitating green emission.

characterization clearly indicated the formation of more compact, dense β-Ga_2O_3 with a smooth interface structure.

It is very clear from the cross-sectional morphology that, with increasing temperature, there is a clear reduction of the film thickness. The higher outdiffusion rate of impinged adatoms with increasing substrate temperature explains the lower film thickness with higher T_s. There is no evidence of Ga atom back-etching of the Si substrate or interdiffusion through the interfacial layer. So, the density of the initial nucleation centers is free from any additional factors other than incoming adatoms, substrate temperature, and oxygen pressure. The chemical analyses (not shown) made using XPS indicate that, in all of the samples deposited under variable temperature, the Ga ions exist in their highest oxidation state (Ga^{3+}). The chemical stoichiometry is well maintained, with a O/Ga ratio close to the expected value (~1.5) in all of the samples.

The β-Ga_2O_3 film on the Si substrate is typically opaque in the UV-to-visible region; therefore, we relied on optical reflectivity measurements for further analysis, especially to determine the band gap. To calculate the band gap of the Ga_2O_3 films, we adopted an indirect approach, which was quite successful in semiconductors. The optical data of PLD Ga_2O_3 films are shown in Figure 4. The room temperature diffuse reflectance (R) of as-deposited PLD Ga_2O_3 films (Figure 4a) was analyzed with the help of the Kubelka−Munk function, which is defined as

$$F(R) = \frac{K}{S} = \frac{(1-R)^2}{2R} \tag{1}$$

Here, $F(R)$ represents the Kubelka−Munk function, which replicates patterns similar to those of wavelength-dependent absorbance of the thin film, and K, S, and R are the absorption coefficient, scattering coefficient, and reflectance, respectively. Figure 4b represents the corresponding wavelength-dependent $F(R)$ plots for each sample. Additionally, a modified Tauc equation has been implemented to calculate the band gap of nanocolumnar β-Ga_2O_3 films.

$$\alpha h\nu = A(h\nu - E_g)^n \tag{2}$$

$$F(R)\, h\nu = A(h\nu - E_g)^n \tag{3}$$

Here, α, h, ν, E_g, $F(R)$, and A represent the absorption coefficient, Planck's constant, incident photon frequency, optical band gap, Kubelka−Munk function, and fitting constant, respectively. We used $n = {}^1/_2$ for calculating the allowed direct transition energy in the electronic band structure (Figure 4c). From the high end (600 °C) to low end (25 °C) of T_s, the band-edge absorption shows a direct shift (Figure 4c). In addition, the increment in the interference fringes (Figure 4a,b) also shows an inverse correlation with T_s. A higher number of interference fringes, especially for samples deposited at lower T_s, infers a higher film thickness, which is further confirmed by the TEM data and analyses. The optical band gap of nanocrystalline PLD Ga_2O_3 films (Figure 4d) is almost similar to that reported for Ga_2O_3; however, the band-gap values were low for amorphous PLD Ga_2O_3 films. This observation refers to the formation of very high quality nanocrystalline PLD Ga_2O_3 films. The presence of a higher defect density, random orientation of unit cells, interstitial states, surface states, cumulative strain, etc., in amorphous samples deviates the band-to-band transition from its ideal value,[27] whereas a high-quality nanocrystalline Ga_2O_3 film with reduced parasitic components leans toward its ideal optical behavior.

The PL spectra of amorphous and nanocrystalline PLD Ga_2O_3 films are presented in Figure 5a and 5c, respectively. The data are shown in association with the corresponding carrier dynamics of photogenerated carriers (Figure 5b,d), respectively. It is clear that all of the possible luminescence transitions are from the donor−acceptor pair, which is strongly supported by the findings of many researchers.[25−27] These are Ga- and O-related states. Although we try to excite all of the samples with near-band-gap photons, there is no such signature of band-to-band transition in these samples. The room temperature deposited PLD Ga_2O_3 films do not show any luminescence signal because most of the excited carriers are

https://doi.org/10.1021/acsanm.1c00378
ACS Appl. Nano Mater. 2021, 4, 3331−3338

being trapped. Additionally, there is an overall blue shift of the PL peak with a significant increment of the absolute intensity. Sufficient surface energy and oxygen over pressure, during deposition, promote the samples with higher substrate temperature to form a close-compact nanocolumnar β-Ga_2O_3 thin film. The overall dimensions of the Ga_2O_3 nanocrystals are much higher than the corresponding Bohr radii and do not have any quantum confinement effect. However, these donor−acceptor pairs are acting as a band of energy states between the valence and conduction bands and can be tuned depending on a few selective deposition parameters, like the substrate temperature, oxygen overpressure, and laser pulse frequency. Also, a phonon is acting as a core member of this downward carrier transition, resulting in a higher photogenerated carrier lifetime. The overall carrier dynamics of both amorphous and nanocrystalline Ga_2O_3 thin films is demonstrated through Figure 5b,d, where horizontal arrows represent photon incidence or photon extraction, vertical arrows represent the generation and recombination of an electron−hole pair, diagonal arrows represent phonon-assisted relaxation of photogenerated carriers, and finally vertical downward arrows (color: dark gray) represent the trapping of carriers. The line thickness of each arrow carries the signature of the corresponding process. The a-Ga_2O_3 thin film suffers from a humongous amount of crystalline defects and is more prone to optical defect formation, which is further affected with surface states. Assertively, the trapping of carriers is dominating the direct carrier recombination through sub-bands. Thus, it shows a very low luminescence intensity (the gray arrow is thick, while others are very thin, except the photon-incident- and photogeneration-related signatures). As we optimize the growth process to obtain a nanocrystalline Ga_2O_3 thin film, decorated with nanocolumnar crystal formation in addition to conical surface morphology, the film becomes more immune to the defect formation. As a result, it shows a much higher percentage of direct recombination of photogenerated carriers, with little carrier trapping. Figure 5d supports the same.

The mechanistic aspects and underlying science behind the observed green emission and wide-range spectral selectivity in intrinsic, nanocrystalline β-Ga_2O_3 films can be explained as follows. We believe that the selectively and precisely engineered nanocrystalline Ga_2O_3 with control over the size, phase, and interface nanostructure is the key aspect that promotes the enhanced PL activity in these samples. As revealed by the AFM studies, self-assembled conical nanotextures with uniform distribution characteristics and roughness on the front surface promote the algorithm of multiple reflection and absorption, which promotes enhanced photon absorption. Deriving such an enhanced property and performance in this work is facilitated by direct control over the growth process. The physical and/or thermodynamic parameters that control the growth and evolution of PLD β-Ga_2O_3 films on Si are the substrate temperature, chamber pressure, laser wavelength, laser power, laser pulse frequency, and distance between the substrate and target source. All of the β-Ga_2O_3 thin-film samples deposited at T_s < 600 °C are all amorphous in nature, which is certainly expected because T_s is lower than the critical temperature for crystallization of Ga_2O_3. At and beyond 600 °C, it shows a particular β-Ga_2O_3 phase with a close-compact nanocolumnar thin film, decorated with nanocrystalline surface morphology. The growth dynamics here are reminiscent of the Structure-Zone Model (SZM)[28] but in a slightly modified way. The original theory was developed on the basis of sputter deposition of different metallic thin films with varying substrate temperature and chamber pressure, whereas here we have deposited complex metal oxide through PLD. The pulsed-laser-generated plume creates a higher order of the localized supersaturating regime on the substrate, and ∼50 mTorr oxygen background pressure drastically reduces the surface adatom mobility, resulting in a very high density of the nucleation centers, compared to the standard sputter-deposited β-Ga_2O_3. Thus, the growth mode of β-Ga_2O_3 films clearly falls into the high-pressure zone-T region in SZM. Therefore, undoubtedly, the compact nanocolumnar β-Ga_2O_3 film, as reflected in the cross-sectional TEM studies, can be due to the growth dynamics.

Additionally, anisotropic thermal conductivity[8,9] plays a significant role during the growth process. The high-temperature (600−700 °C) PLD-assisted formation of a β-Ga_2O_3 nanocrystalline thin film on Si has been organized in two consecutive stages: initial random crystallization of β-Ga_2O_3 on amorphous SiO_2, followed by thermally driven preferred surface diffusion and crystallization of a nanocolumnar (Figure 5e) structure (Figure 5f, showing the schematic). Luo et al.[9] have already shown differential thermal conductivity toward different orientations of β-Ga_2O_3 crystals. Correlating that observation with the current growth process, we can infer that the first step is almost random, resulting in nanocrystallization with all possible orientations. Then, at the beginning of the second stage, higher thermally conductive zones promote better kinetic energy to the incoming adatoms, whereas the others appear to be relatively dull for providing sufficient energy. As a result, the incoming adatoms tend to settle down at those lower-energy spots, forming compact vertical nanocolumns. This is similar to the GLAD process[29,30] but without any external shadowing effect. Assertively, it shows close-compact nanocolumnar growth with a higher fill factor. Thus, the observed enhanced green-emission PL characteristics in the intrinsic nanocrystalline Ga_2O_3 films without the need for any dopants are attributed to precise engineering with control over the size, phase, and interface nanostructure, where the self-assembled conical nanotextures promote the algorithm of multiple reflection and absorption, leading to such optoelectronic properties.

CONCLUSIONS

Summarizing the results, we demonstrated an approach based on selective engineering of the size-, phase-, and interface-nanostructure-controlled β-Ga_2O_3 films to realize reliable and highly intense green-emission PL without the need for expensive processing, epitaxial system, and dopants. In nanocrystalline β-Ga_2O_3 films with an average crystallite size of ∼9 nm, the green-emission PL noted is remarkable and is extremely high (∼30 times). Structural and interface-nanostructure analyses indicate that high-quality nanocrystalline β-Ga_2O_3 films with highly dense and interconnected nanocolumnar structures promote enhanced optoelectronic performance. We believe that there may be further options available to further tune and improve the optoelectronic performance, while the underlying science and mechanisms may be applicable to a large class of wide-band-gap nanostructured oxides for optical, electronic, and optoelectronic devices for extreme environment applications.

https://doi.org/10.1021/acsanm.1c00378
ACS Appl. Nano Mater. 2021, 4, 3331−3338

AUTHOR INFORMATION

Corresponding Authors

Susheng Tan − *Department of Electrical and Computer Engineering and Petersen Institute of NanoScience and Engineering, University of Pittsburgh, Pittsburgh, Pennsylvania 15261, United States;* orcid.org/0000-0002-6162-7443; Email: sut6@pitt.edu

C. V. Ramana − *Center for Advanced Materials Research and Department of Mechanical Engineering, University of Texas at El Paso, El Paso, Texas 79968, United States;* orcid.org/0000-0002-5286-3065; Email: rvchintalapalle@utep.edu

Authors

Nanthakishore Makeswaran − *Center for Advanced Materials Research and Department of Mechanical Engineering, University of Texas at El Paso, El Paso, Texas 79968, United States*

Debabrata Das − *Center for Advanced Materials Research, University of Texas at El Paso, El Paso, Texas 79968, United States;* orcid.org/0000-0003-4326-6805

Vishal Zade − *Center for Advanced Materials Research and Department of Mechanical Engineering, University of Texas at El Paso, El Paso, Texas 79968, United States; Center for Integrated Nano Technologies, Sandia National Laboratory, Albuquerque, New Mexico 87185, United States*

Paul Gaurav − *Center for Advanced Materials Research and Department of Mechanical Engineering, University of Texas at El Paso, El Paso, Texas 79968, United States*

V. Shutthanandan − *Environmental Molecular Sciences Laboratory (EMSL), Pacific Northwest National Laboratory (PNNL), Richland, Washington 99352, United States;* orcid.org/0000-0003-2957-7535

Complete contact information is available at: https://pubs.acs.org/10.1021/acsanm.1c00378

Notes

The authors declare no competing financial interest.

ACKNOWLEDGMENTS

This material is based upon work supported by the Air Force Office of Scientific Research under Award FA9550-18-1-0387. However, any opinions, finding, and conclusions or recommendations expressed in this material are those of the author(s) and do not necessarily reflect the views of the United States Air Force. The authors also acknowledge, with pleasure, support from the National Science Foundation (NSF) through NSF-PREM Grant DMR-1827745. A portion of the research (XPS measurements) was performed using EMSL, a national scientific user facility sponsored by the Department of Energy's Office of Biological and Environmental Research and located at PNNL.

REFERENCES

(1) Rubio, E. J.; Mates, T. E.; Manandhar, S.; Nandasiri, M.; Shutthanandan, V.; Ramana, C. V. Tungsten Incorporation into Gallium Oxide: Crystal Structure, Surface and Interface Chemistry, Thermal Stability, and Interdiffusion. *J. Phys. Chem. C* **2016**, *120*, 26720−26735.

(2) Lin, R.; Zheng, W.; Zhang, D.; Zhang, Z.; Liao, Q.; Yang, L.; Huang, F. High-Performance Graphene/β-Ga_2O_3 Heterojunction Deep-Ultraviolet Photodetector with Hot-Electron Excited Carrier Multiplication. *ACS Appl. Mater. Interfaces* **2018**, *10*, 22419−22426.

(3) Arora, K.; Goel, N.; Kumar, M.; Kumar, M. Ultrahigh Performance of Self-Powered β-Ga_2O_3 Thin Film Solar-Blind Photodetector Grown on Cost-Effective Si Substrate Using High-Temperature Seed Layer. *ACS Photonics* **2018**, *5*, 2391−2401.

(4) Zhang, W.; Naidu, B. S.; Ou, J. Z.; O'Mullane, A. P.; Chrimes, A. F.; Carey, B. J.; Wang, Y.; Tang, S. Y.; Sivan, V.; Mitchell, A.; Bhargava, S. K.; Kalantar-zadeh, K. Liquid Metal/Metal Oxide Frameworks with Incorporated Ga_2O_3 for Photocatalysis. *ACS Appl. Mater. Interfaces* **2015**, *7*, 1943−1948.

(5) Oh, S.; Kim, C.-K.; Kim, J. High Responsivity β-Ga_2O_3 Metal−Semiconductor−Metal Solar-Blind Photodetectors with Ultraviolet Transparent Graphene Electrodes. *ACS Photonics* **2018**, *5*, 1123−1128.

(6) Qian, L.-X.; Wu, Z.-H.; Zhang, Yi-Yu; Lai, P. T.; Liu, X.-Z.; Li, Y.-R. Ultrahigh-Responsivity, Rapid-Recovery, Solar-Blind Photodetector Based on Highly Nonstoichiometric Amorphous Gallium Oxide. *ACS Photonics* **2017**, *4*, 2203−2211.

(7) Mezzadri, F.; Calestani, G.; Boschi, F.; Delmonte, D.; Bosi, M.; Fornari, R. Crystal Structure and Ferroelectric Properties of ϵ-Ga_2O_3 Films Grown on (0001)-Sapphire. *Inorg. Chem.* **2016**, *55*, 12079−12084.

(8) Pearton, S. J.; Yang, J.; Cary, P. H.; Ren, F.; Kim, J.; Tadjer, M. J.; Mastro, M. A. A review of Ga_2O_3 materials, processing, and devices. *Appl. Phys. Rev.* **2018**, *5*, 011301.

(9) Guo, Z.; Verma, A.; Wu, X.; Sun, F.; Hickman, A.; Masui, T.; Kuramata, A.; Higashiwaki, M.; Jena, D.; Luo, T. Anisotropic thermal conductivity in single crystal β-gallium oxide. *Appl. Phys. Lett.* **2015**, *106*, 111909.

(10) Pang, R.; Teramura, K.; Morishita, M.; Asakura, H.; Hosokawa, S.; Tanaka, T. Enhanced CO evolution for photocatalytic conversion of CO_2 by H_2O over Ca modified Ga_2O_3. *Commun. Chem.* **2020**, *3*, 137.

(11) Harada, T.; Ito, S.; Tsukazaki, A. Electric dipole effect in $PdCoO_2$/β-Ga_2O_3 Schottky diodes for high-temperature operation. *Sci. Adv.* **2019**, *5*, 5733.

(12) Kim, J.; Mastro, M. A.; Tadjer, M. J.; Kim, J. Heterostructure WSe_2-Ga_2O_3 Junction Field-Effect Transistor for Low-Dimensional High-Power Electronics. *ACS Appl. Mater. Interfaces* **2018**, *10*, 29724−29729.

(13) Liang, H.; Cui, S.; Su, R.; Guan, P.; He, Y.; Yang, L.; Chen, L.; Zhang, Y.; Mei, Z.; Du, X. Flexible X-ray Detectors Based on Amorphous Ga_2O_3 Thin Films. *ACS Photonics* **2019**, *6*, 351−359.

(14) Li, K. H.; Alfaraj, N.; Kang, C. H.; Braic, L.; Hedhili, M. N.; Guo, Z.; Ng, T. K.; Ooi, B. S. Deep-Ultraviolet Photodetection Using Single-Crystalline β-Ga_2O_3/NiO Heterojunctions. *ACS Appl. Mater. Interfaces* **2019**, *11*, 35095−35104.

(15) Yang, G.; Jang, S.; Ren, F.; Pearton, S. J.; Kim, J. Influence of High-Energy Proton Irradiation on β-Ga_2O_3 Nanobelt Field-Effect Transistors. *ACS Appl. Mater. Interfaces* **2017**, *9*, 40471−40476.

(16) Anhar Uddin Bhuiyan, A. F. M.; Feng, Z.; Johnson, J. M.; Huang, H. L.; Hwang, J.; Zhao, H. MOCVD Epitaxy of Ultrawide Bandgap β-$(Al_xGa_{1-x})_2O_3$ with High-Al Composition on (100) β-Ga_2O_3 Substrates. *Cryst. Growth Des.* **2020**, *20*, 6722−6730.

(17) Pratiyush, A. S.; Krishnamoorthy, S.; Kumar, S.; Xia, Z.; Muralidharan, R.; Rajan, S.; Nath, D. N. Demonstration of zero bias responsivity in MBE grown β-Ga_2O_3 lateral deep-UV photodetector. *Jpn. J. Appl. Phys.* **2018**, *57*, 060313.

(18) Park, S.; Yoon, H. J. New Approach for large-area thermoelectric junctions with a liquid eutectic gallium−indium electrode. *Nano Lett.* **2018**, *18*, 7715−7718.

(19) Simeone, F. C.; Yoon, H. J.; Thuo, M. M.; Barber, J. R.; Smith, B.; Whitesides, G. M. Defining the value of injection current and effective electrical contact area for EGaIn-based molecular tunneling junctions. *J. Am. Chem. Soc.* **2013**, *135*, 18131−18144.

(20) Um, H. J.; Kong, G. D.; Yoon, H. J. Thermally Controlled Phase Transition of Low-Melting Electrode for Wetting-Based Spontaneous Top Contact in Molecular Tunnel Junction. *ACS Appl. Mater. Interfaces* **2018**, *10*, 34758−34764.

(21) HOU, Y.; WANG, X.; WU, L.; DING, Z.; FU, X. Efficient Decomposition of Benzene over a β-Ga_2O_3 Photocatalyst under Ambient Conditions. *Environ. Sci. Technol.* **2006**, *40*, 5799−5803.
(22) Kim, S.; Oh, S.; Kim, J. Ultrahigh Deep-UV Sensitivity in Graphene-Gated β-Ga_2O_3 Phototransistors. *ACS Photonics* **2019**, *6*, 1026−1032.
(23) Pozina, G.; Forsberg, M.; Kaliteevski, M. A.; Hemmingsson, C. Emission properties of Ga_2O_3 nano-flakes: effect of excitation density. *Sci. Rep.* **2017**, *7*, 42132.
(24) Wang, Y.; Dickens, P. T.; Varley, J. B.; Ni, X.; Lotubai, E.; Sprawls, S.; Liu, F.; Lordi, V.; Krishnamoorthy, S.; Blair, S.; Lynn, K. G.; Scarpulla, M.; Sensale-Rodriguez, B. Incident wavelength and polarization dependence of spectral shifts in β-Ga_2O_3 UV photoluminescence. *Sci. Rep.* **2018**, *8*, 18075.
(25) Huso, J.; McCluskey, M. D.; Yu, Y.; Islam, M. M.; Selim, F. Localized UV emitters on the surface of β-Ga_2O_3. *Sci. Rep.* **2020**, *10*, 21022.
(26) Cho, J. B.; Jung, G.; Kim, K.; Kim, J.; Hong, S.-K.; Song, J.-H.; Jang, J. I. Highly Asymmetric Optical Properties of β-Ga_2O_3 as Probed by Linear and Nonlinear Optical Excitation Spectroscopy. *J. Phys. Chem. C* **2021**, *125*, 1432−1440.
(27) Zhou, X. T.; Heigl, F.; Ko, J. Y. P.; Murphy, M. W.; Zhou, J. G.; Regier, T.; Blyth, R. I. R.; Sham, T. K. Origin of luminescence from Ga_2O_3 nanostructures studied using x-ray absorption and luminescence spectroscopy. *Phys. Rev. B: Condens. Matter Mater. Phys.* **2007**, *75*, 125303.
(28) Mirica, E.; Kowach, G.; Du, H. Modified Structure Zone Model to Describe the Morphological Evolution of ZnO Thin Films Deposited by Reactive Sputtering. *Cryst. Growth Des.* **2004**, *4*, 157−159.
(29) Tripathi, A.; Harris, K. D.; Elias, A. L. Peroxidase-Like Behavior of Ni Thin Films Deposited by Glancing Angle Deposition for Enzyme-Free Uric Acid Sensing. *ACS omega* **2020**, *5*, 9123−9130.
(30) Krishnan, R.; Lu, T. M.; Koratkar, N. Functionally strain-graded nanoscoops for high power Li-ion battery anodes. *Nano Lett.* **2011**, *11*, 377−84.

https://doi.org/10.1021/acsanm.1c00378
ACS Appl. Nano Mater. 2021, 4, 3331−3338